Semi-Analytical Approach to
Four-Fermion Production in e^+e^- Annihilation [†]

D. Bardin [1,2],   M. Bilenky [2,3],   D. Lehner [3],
A. Olchevski [2,a]   and   T. Riemann [3]

[1] Theory Division, CERN, CH–1211, Geneva 23, Switzerland
[2] Joint Institute for Nuclear Research, ul. Joliot Curie 6,
RU–141980 Dubna, Moscow Region, Russia
[3] DESY–Institut für Hochenergiephysik, Platanenallee 6, D–15738 Zeuthen, Germany

ABSTRACT

A study of the semi-analytical approach to four-fermion production in e^+e^- annihilation is presented. We classify all possible four-fermion final states and present results of new calculations for the 'basic' processes with the WW, ZZ, and ZH off-shell production together with some examples of 'background' processes. The Initial State Radiative corrections are included for the basic processes. Several numerical examples are given in the energy range from LEP 2 up to $\sqrt{s} = 1$ TeV.

Contribution to the Proceedings of the
Zeuthen Workshop on Elementary Particle Theory – Physics at LEP200 and Beyond,
Teupitz, Germany, 10–15 April, 1994.

[†] Talk presented by D. Bardin.
[a] Present address: PPE Division, CERN.

email: BARDINDY@CERNVM.CERN.CH, bilenky@hades.ifh.de,
         LEHNER@CONVEX.IFH.DE, OLSHEVSK@VXCERN.CERN.CH,
         RIEMANN@CERNVM.CERN.CH

HEP-PH-9406340

1   INTRODUCTION

While at LEP 1 the basic process is two-fermion production via a single Z-boson (or photon) exchange, at LEP 2 the typical process will be the 'double-resonance' production of four-fermion final states. LEP 2 will operate just in the threshold region of W- or Z-pair production and, if the Higgs-boson mass fulfils $60 \leq M_H \leq 100$ GeV, of ZH production. Already in the tree level approximation, the double-resonance physics is much richer and much more interesting and complex than the single Z-boson production.

A specific four-fermion final state can be produced by many Feynman diagrams with many possible virtual states, including all the carriers of fermion interactions in the Standard Model: $\gamma, Z, W^{\pm}, g$, and H. We will distinguish between 'basic' diagrams, which contain two potentially resonating virtual states (W, Z, H) in the s-channel and 'background' diagrams, which are just the rest. The general topology of the basic diagrams is shown in figure 1. The contribution of background diagrams to a given final state is usually suppressed. Some background diagrams for W-pair production are given in figure 2.

The analytical result for the Born on-shell W-pair production has been known for long in the literature [1][1]. The off-shell case was treated in [3]. A calculation of off-shell Z-pair production was done in [4].

In this paper we present semi-analytical results for off-shell production of bosonic pairs (WW, ZZ, ZH) including universal lowest-order Initial State Radiative (ISR) corrections with soft-photon exponentiation. For the case of W-pairs, we also present results with complete $\mathcal{O}(\alpha)$ ISR corrections and some examples of four-fermion background processes.

The paper is organized as follows: In the next section, we classify the four-fermion production processes in $e^+ e^-$ annihilation. In section 3 we introduce the notations and present the formulae for the basic processes. In section 4, the contributions of the background diagrams to the simplest final state are characterized. The ISR corrections are described in section 5. In section 6, we present concluding remarks and prospects.

2   A   CLASSIFICATION   OF   FOUR-FERMION   PROCESSES

In this section we will classify the four-fermion production in the Standard Model [2]. The number of Feynman diagrams depends crucially on the final state. In general all possible final states can be subdivided into two classes.

The first class comprises production of up (anti-up) and anti-down (down) fermion pairs,

$$(U_i \ \bar{D}_i) \ + \ (D_j \ \bar{U}_j) \,,$$

where i, j are generation indices. The final states produced via virtual W-pairs belong to this class. We will call these 'CC' type final states. The second class is the production of

---

[1]Some approximate results on the analytical treatment of off-shell W-pair production near threshold can be found in [2].

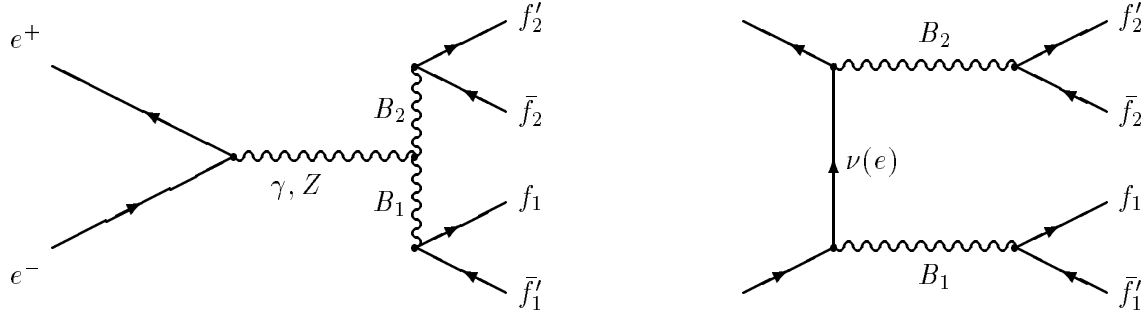[2]The classification is done with the use of CompHEP [5].

Figure 1: The basic contributions to off-shell boson-pair production: `crayfish` and `crab`; $B = W^{\pm}, Z, H$.

two fermion-antifermion pairs,

$$(f_i \ \bar{f}_i) \ + \ (f_j \ \bar{f}_j) \, , f = U, \ D.$$

As it is produced via a pair of two virtual neutral vector bosons we will call this a final state of the 'NC' type. Obviously these two classes overlap for certain final states.

The number of Feynman diagrams in the 'CC' class is shown in table 1. Three different cases occur in the table:

	$\bar{d}u$	$\bar{s}c$	$\bar{e}\nu_e$	$\bar{\mu}\nu_\mu$	$\bar{\tau}\nu_\tau$
$d\bar{u}$	*43*	**11**	20	**10**	**10**
$e\bar{\nu}_e$	20	20	*56*	18	18
$\mu\bar{\nu}_\mu$	**10**	**10**	18	*19*	9

Table 1: Number of Feynman diagrams contributing to the production of 'CC' type final states.

(i) The two produced fermion pairs are different $(i \neq j)$ and the final state does not contain an $e^{\pm}$ (numbers in **boldface**). For this case, the number of diagrams varies between 9 and 11, depending on the final state's neutrino content. The background diagrams for this simplest case are shown in figure 2.

(ii) The four-fermion final state contains one $e\bar{\nu}_e$- or $\bar{e}\nu_e$-pair (roman numbers); the number of diagrams grows to 18, 19 or 20, due to the additional t-channel exchange diagrams.

(iii) Two mutually charge-conjugated fermion pairs $(i = j)$ are produced (*italic* numbers). Here, the diagrams may contain neutral-boson $(Z, \gamma, H, \text{gluon})$ exchanges. One should emphasize that this overlaps the 'NC' classification.

For the final states corresponding to the 'NC' class the number of Feynman diagrams is presented in table 2:
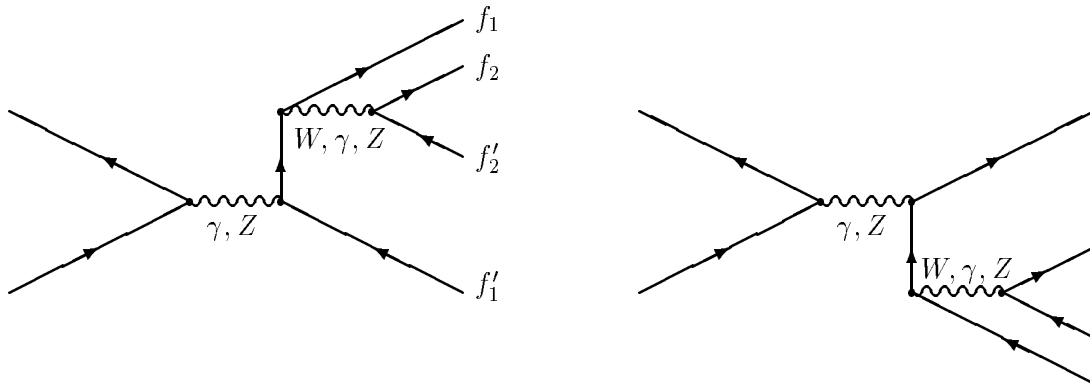
Figure 2: Background contributions to off-shell W-pair production: up and down `reindeers`.

(i) The simplest case (numbers in **boldface**) does not contain electrons or identical fermions[3].

(ii) With identical fermions f ($f \neq e, \nu_e$), the number of diagrams (in `typewriter`) grows drastically, since it is necessary to satisfy the Pauli principle (i.e. to antisymmetrize the amplitude).

(iii) The numbers in romans correspond to the final states that include $f = e, \nu_e$ except those covered by item (iv). The large number of diagrams here is due to additional t-channel diagrams.

(iv) The numbers in *italics* correspond to final states that are also present in table 1, case (iii). The basic diagrams proceed via both WW- and ZZ-exchanges.

So far we have investigated semi-analytically only the two simplest cases of the 'CC' and the 'NC' classifications. In section 4 we will present the production of two different fermion pairs:

$$e^+e^- \rightarrow (W^+W^-, W^{\pm}\bar{f}f') \rightarrow \bar{f}'_1 f_1 f'_2 \bar{f}_2,$$
$$f_i, f'_j \neq e, \nu_e .$$

An example of the 'NC' type process with 24 Feynman diagrams (case (i) of table 2) will be discussed in another contribution to this conference [6]. For the more involved processes, especially for case (ii) of table 1 with final states containing an $e\bar{\nu}_e$ pair, investigations have been started. We expect that the topologies indicated with roman numbers may also be treated by our method.

Another classification of four-fermion processes was presented recently [7]. This reference separates leptonic, semileptonic, and hadronic four-fermion final states. For leptonic processes they agree with our number of Feynman diagrams. For semileptonic processes agreement is found in all cases but one, namely $q\bar{q}\nu_e\bar{\nu}_e$. The authors of [7] have 19 diagrams instead of our 21 for this case. The explanation is that for this process a W-fusion diagram exists, where two W-bosons produce a $q\bar{q}$ state with a virtual q' in the t-channel.

---

[3]We exclude the Higgs-boson exchange diagrams from the classification in the tables.

	$\bar{d}d$	$\bar{u}u$	$\bar{e}e$	$\bar{\mu}\mu$	$\bar{\nu}_e\nu_e$	$\bar{\nu}_\mu\nu_\mu$
$\bar{d}d$	4·16	*43*	48	**24**	21	**10**
$\bar{s}s$	**32**	*43*	48	**24**	21	**10**
$\bar{u}u$	*43*	4·16	48	**24**	21	**10**
$\bar{e}e$	48	48	4·36	48	*56*	20
$\bar{\mu}\mu$	**24**	**24**	48	4·12	19	*19*
$\bar{\tau}\tau$	**24**	**24**	48	**24**	19	**10**
$\bar{\nu}_e\nu_e$	21	21	*56*	19	4·9	12
$\bar{\nu}_\mu\nu_\mu$	**10**	**10**	20	*19*	12	4·3
$\bar{\nu}_\tau\nu_\tau$	**10**	**10**	20	**10**	12	**6**

Table 2: Number of Feynman diagrams contributing to the 'NC' type production of two fermions pairs.

For a given q, say d, q' may be u, c or t (due to Cabibbo-Kobayashi-Maskawa mixing). In our classification we count all three diagrams, while in [7] this is counted only once. Finally, for hadronic processes we agree only in one of seven cases, namely in our example with 11 diagrams. The reasons for these differences are twofold. Firstly, once more, quark mixing is neglected in [7]. Secondly, we count gluon-exchange diagrams while this is not done in [7]. Taking these differences into account, both classifications agree.

At the end of this section we introduce some notations. Background diagrams may contain one resonating virtual s-channel state or none (non-resonating background). We will denote by a sub-index n the total number of resonating s-channel propagators in a separate contribution σ_n to the cross-section of four-fermion production,

$$e^+e^- \rightarrow (W^+W^-, ZZ, ZH, \ldots) \rightarrow 4f.$$

Therefore, the basic contributions carry sub-index 4, the background-basic interferences 3 or 2, and the pure background contributions have sub-index 2, 1 or 0. With appropriate kinematical cuts, certain resonating states may be selected and contributions with indices 4, 3, 2, 1, and 0 should be hierarchically less and less important.

3 BASIC CROSS-SECTIONS

Here we present the basic cross-section formulae for the three cases described by the diagrams of figure 1 with WW, ZZ, and ZH intermediate states. They all may be expressed by twofold convolutions of a hard-scattering off-shell cross-section with Breit-Wigner density functions. For the WW case, this representation was invented in [3]:

$$\sigma^{WW}(s) = \int_0^s ds_1\, \rho_W(s_1) \int_0^{(\sqrt{s}-\sqrt{s_1})^2} ds_2\, \rho_W(s_2)$$
$$\times\, \sigma_4^{WW}(s; s_1, s_2), \tag{1}$$

where

$$\rho_W(s_i) = \frac{1}{\pi} \frac{\sqrt{s_i}\,\Gamma_W(s_i) \times \mathrm{BR}(i)}{|s_i - M_W^2 + i\sqrt{s_i}\,\Gamma_W(s_i)|^2} \tag{2}$$

is the Breit-Wigner density function originating from the $W^\pm$ s-channel propagators and $\mathrm{BR}(i)$ is the corresponding branching ratio. Similar densities ρ_Z and ρ_H associated with Z (H) s-channel exchanges can be obtained by the replacements $M_W, \Gamma_W \rightarrow M_Z, \Gamma_Z; (M_H, \Gamma_H)$. They are normalized so that

$$\rho_B(s) \overset{\Gamma_B \to 0}{\longrightarrow} \delta(s - M_B) \times \mathrm{BR}(i), B = W, Z, H. \tag{3}$$

Further,

$$\Gamma_W(s) = \frac{G_\mu M_W^2}{6\pi\sqrt{2}} \sqrt{s} \sum_f N_c(f) \tag{4}$$

is the off-shell (s-dependent) W-width and $N_c(f){=}1(3)$ for leptons(quarks). The sum in (4) extends over all open fermion channels. At extremely high energies, additionally opening channels may substantially contribute to $\Gamma_W(s)$.

The cross-section $\sigma_4^{WW}(s, s_1, s_2)$ contains six pieces but is described by only three functions $\mathcal{G}_4^a(s; s_1, s_2)$, which are different for the s- and t-channel and the st-interference:

$$\sigma_4^{WW}(s; s_1, s_2) =$$
$$\frac{(G_\mu M_W^2)^2}{8\pi s} \left[\left(c_{\gamma\gamma} + c_{\gamma Z} + c_{ZZ} \right) \mathcal{G}_4^s(s; s_1, s_2) \right.$$
$$+ \ (c_{\nu\gamma} + c_{\nu Z})\,\mathcal{G}_4^{st}(s; s_1, s_2)$$
$$\left. + \ c_{\nu\nu}\mathcal{G}_4^t(s; s_1, s_2) \right]. \tag{5}$$

The coefficients $c_{\alpha\beta}$ consist of $Z(\gamma)ee$- and $Z(\gamma)WW$-couplings and γ, Z-propagator ratios:

$$
\begin{aligned}
c_{\gamma\gamma} &= 8s_W^4\, Q_e^2, \\
c_{\gamma Z} &= 4s_W^2\, v_e\, |Q_e|\, \Re e \frac{s}{s - M_Z^2 + iM_Z\Gamma_Z(s)}, \\
c_{ZZ} &= \frac{1}{2}\left(v_e^2 + a_e^2\right)\left| \frac{s}{s - M_Z^2 + iM_Z\Gamma_Z(s)} \right|^2, \\
c_{\nu\gamma} &= -4s_W^2\, |Q_e|, \\
c_{\nu Z} &= -(v_e + a_e)\,\Re e \frac{s}{s - M_Z^2 + iM_Z\Gamma_Z(s)}, \\
c_{\nu\nu} &= 1,
\end{aligned}
\tag{6}
$$

with $Q_e = -1, a_e = 1, v_e = 1 - 4s_W^2, s_W^2 = \sin^2\theta_W$. The three irreducible kinematical functions are

$$\mathcal{G}_4^s(s; s_1, s_2) = \frac{\lambda^{3/2}}{s^3 s_1 s_2}\left[\frac{\lambda}{6} + 2s(s_1 + s_2) + 2s_1 s_2\right],$$

$$\mathcal{G}_4^{\mathrm{st}}(s; s_1, s_2) = \frac{\lambda^{1/2}}{s^2 s_1 s_2} \left\{ \frac{\lambda}{6} \left[s + 11(s_1 + s_2) \right] \right.$$
$$+ 2s \left(s_1^2 + 3 s_1 s_2 + s_2^2 \right) - 2 \left(s_1^3 + s_2^3 \right)$$
$$\left. - 4 s_1 s_2 \left[s(s_1 + s_2) + s_1 s_2 \right] \mathcal{L}_4 \right\},$$

$$\mathcal{G}_4^{\mathrm{t}}(s; s_1, s_2) = \frac{\lambda^{1/2}}{s s_1 s_2} \left[\frac{\lambda}{6} + 2s(s_1 + s_2) \right.$$
$$\left. - 8 s_1 s_2 + 4 s_1 s_2 (s - s_1 - s_2) \mathcal{L}_4 \right], \tag{7}$$

with

$$\lambda \equiv \lambda(s; s_1, s_2)$$
$$= s^2 + s_1^2 + s_2^2 - 2 s s_1 - 2 s_1 s_2 - 2 s_2 s \tag{8}$$

and

$$\mathcal{L}_4(s; s_1, s_2) = \frac{1}{\sqrt{\lambda}} \ln \frac{s - s_1 - s_2 + \sqrt{\lambda}}{s - s_1 - s_2 - \sqrt{\lambda}} . \tag{9}$$

In the limit (3), the on-shell W-pair production cross-section is obtained as given in [1]. The corresponding set of formulae for basic off-shell ZZ production is:

$$\sigma^{ZZ}(s) = \int_0^s ds_1 \, \rho_Z(s_1) \int_0^{(\sqrt{s} - \sqrt{s_1})^2} ds_2 \, \rho_Z(s_2)$$
$$\times \sigma_4^{ZZ}(s; s_1, s_2). \tag{10}$$

The off-shell Z-boson width, which enters the definition of ρ_Z, has the form

$$\Gamma_Z(s) = \frac{G_\mu M_Z^2}{24 \pi \sqrt{2}} \sqrt{s} \sum_f (v_f^2 + a_f^2) N_c(f). \tag{11}$$

The cross-section $\sigma_4^{ZZ}(s, s_1, s_2)$ is extremely compact and can be described by only one function $\mathcal{G}_4^{\mathrm{t+u}}(s; s_1, s_2)$, which is the sum of three others:

$$\mathcal{G}_4^{\mathrm{t+u}}(s; s_1, s_2) = \mathcal{G}_4^{\mathrm{t}}(s; s_1, s_2) + \mathcal{G}_4^{\mathrm{u}}(s; s_1, s_2)$$
$$+ \mathcal{G}_4^{\mathrm{tu}}(s; s_1, s_2). \tag{12}$$

Here the functions $\mathcal{G}_4^{\mathrm{u}}(s; s_1, s_2) = \mathcal{G}_4^{\mathrm{t}}(s; s_2, s_1)$ correspond to u- and t-channel diagrams and $\mathcal{G}_4^{\mathrm{tu}}(s, s_1, s_2)$ describes the tu-interference. The cross-section σ_4^{ZZ} is given by:

$$\sigma_4^{ZZ}(s; s_1, s_2) =$$
$$\frac{(G_\mu M_Z^2)^2}{64 \pi s} (v_e^4 + 6 v_e^2 a_e^2 + a_e^4) \mathcal{G}_4^{\mathrm{t+u}}(s, s_1, s_2) \tag{13}$$

6

with the kinematical function

$$\mathcal{G}_4^{\mathrm{t+u}}(s;s_1,s_2) = \frac{\lambda^{1/2}}{s} \left[\frac{s^2 + (s_1+s_2)^2}{s-s_1-s_2} \mathcal{L}_4 - 2 \right].$$

Finally, the basic off-shell ZH cross-section is:

$$\sigma^{ZH}(s) = \int_0^s ds_1\, \rho_H(s_1) \int_0^{(\sqrt{s}-\sqrt{s_1})^2} ds_2\, \rho_Z(s_2)$$
$$\times\ \sigma_4^{ZH}(s;s_1,s_2). \tag{14}$$

Below the threshold of the decay $H \to W^+W^-$, the off-shell width has the form

$$\Gamma_H(s) = \frac{G_\mu}{4\pi\sqrt{2}} \sqrt{s} \sum_f m_f^2 N_c(f). \tag{15}$$

The cross-section $\sigma_4^{ZH}(s;s_1,s_2)$ is given by

$$\sigma_4^{ZH}(s;s_1,s_2) = \frac{(G_\mu M_Z^2)^2}{96\pi s} \frac{M_Z^2}{s} \left(v_e^2 + a_e^2 \right)$$
$$\times \left| \frac{s}{s - M_Z^2 + iM_Z\Gamma_Z(s)} \right|^2 \mathcal{G}_4^{\mathrm{Bj}}(s;s_1,s_2). \tag{16}$$

Again, it contains only one kinematical function, namely $\mathcal{G}_4^{\mathrm{Bj}}(s;s_1,s_2)$:

$$\mathcal{G}_4^{\mathrm{Bj}}(s;s_1,s_2) = \frac{\lambda^{1/2}}{s^2 s_2} \left(\lambda + 12 s s_2 \right). \tag{17}$$

The energy dependences of the off-shell WW, ZZ, and ZH basic cross-sections are presented in figures 3–5. For comparison we also show on-shell cross-sections for all three cases. With respect to the on-shell case, off-shell cross-sections are substantially reduced in the threshold region and develop tails at high energies so that boson widths cannot be neglected for $s \gg (M_{B_1} + M_{B_2})^2$. Going off-shell, the cross-section peaks are shifted to higher energies. Using constant widths, i.e. $\sqrt{s}\,\Gamma_B(s) \to M_B\Gamma_B$, corresponds to redefinitions of the boson masses [8]: $M_B \to \bar{M}_B = M_B + \frac{1}{2}\Gamma_B^2/M_B$. For the W this results in $\bar{M}_W \approx M_W + 26$ MeV [9]. That lowers the cross-section around threshold by at most $\approx -1.7\%$, while for $\sqrt{s} > 180$ GeV the effect is small and positive ($\leq 0.1\%$). Numerical results were obtained with the Fortran program `GENTLE` [10].

4   BACKGROUND

In this section we briefly sketch our results for the semi-analytical treatment of the process (1), the production of four different fermions excluding electron or electron neutrino (case (i) in table 1). This is described by the basic diagrams of figure 1 and by the eight background diagrams of figure 2. In the unitary gauge, there are no other diagrams for this particular final state. All results were obtained with the help of `FORM` [11], `SCHOONSCHIP` [12], and `CompHEP` [5].
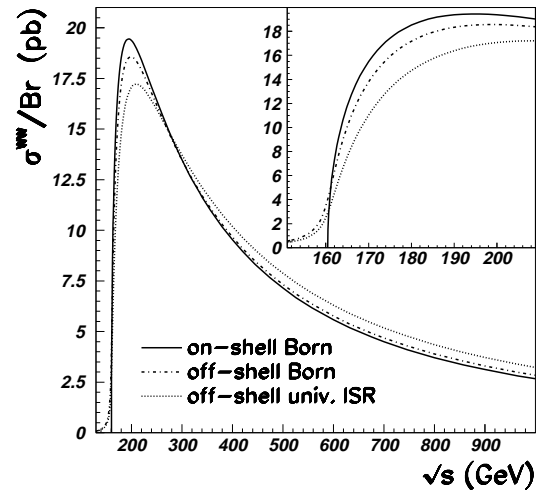
7

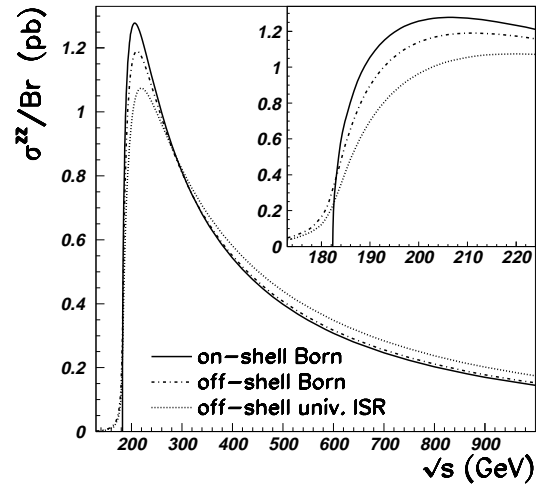Figure 3: The basic W-pair production.

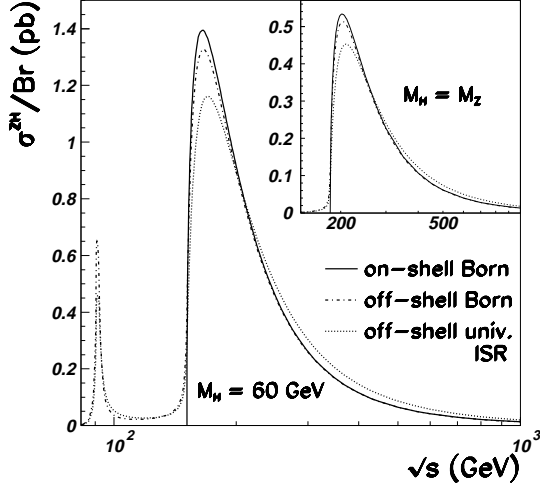Figure 4: The basic Z-pair production.

8

Figure 5: The basic ZH production.

After the analytical integration over five angular variables, one arrives at a doubly-convoluted representation for the cross-section:

$$\sigma^{4f}(s) = \int\limits_0^s ds_1 \rho_W(s_1) \int\limits_0^{(\sqrt{s}-\sqrt{s_1})^2} ds_2 \, \rho_W(s_2)$$
$$\times \left[\sigma_4^{WW}(s; s_1, s_2) + \sigma_3^{4f}(s; s_1, s_2) \right.$$
$$\left. + \sigma_2^{4f}(s; s_1, s_2) \right]. \tag{18}$$

The basic contribution σ_4^{WW} is given by (5). The term σ_2^{4f} corresponds to figure 2 and σ_3^{4f} are interference contributions.

We obtained explicit representations for the cross-sections $\sigma_3^{4f}(s; s_1, s_2)$ and $\sigma_2^{4f}(s; s_1, s_2)$ in terms of seven new kinematical functions (three functions $\mathcal{G}_3^a$ and four functions $\mathcal{G}_2^a$), coupling constants and propagator ratios (similar to (5)). The formulae for the cross-sections themselves are rather appealing, while only three of the kinematical functions are of the same compactness as those of the basic processes. Four interference functions (two $\mathcal{G}_3^a$ and two $\mathcal{G}_2^a$) could be written only with the aid of a cumbersome polynomial presentation of the following type:

$$\mathcal{G}_3^a(s, s_1, s_2) = \sqrt{\lambda} \sum_{i,j=0}^1 \left[s_1 \mathcal{L}_3(s; s_1, s_2) \right]^i$$
$$\times \left[s_1 s_2 \mathcal{L}_4(s; s_1, s_2) \right]^j \mathcal{P}_{ij}^a(s; s_1, s_2), \tag{19}$$

$$\mathcal{G}_2^a(s, s_1, s_2) = \sqrt{\lambda} \sum_{i,j=0}^1 \left[s_1 \mathcal{L}_3(s; s_1, s_2) \right]^i$$
$$\times \left[s_2 \mathcal{L}_3(s; s_2, s_1) \right]^j \mathcal{P}_{ij}^a(s; s_1, s_2), \tag{20}$$

9

$$\mathcal{P}_{ij}^a(s;s_1,s_2) = p_0^a(ij)$$
$$+ \sum_{n=1}^{3} \frac{(s_1 s_2)^{n-1}}{\lambda^n} p_n^a(ij), \tag{21}$$

with $\mathcal{L}_4(s;s_1,s_2)$ given by (9) and

$$\mathcal{L}_3(s;s_1,s_2) = \frac{1}{\sqrt{\lambda}} \ln \frac{s+s_1-s_2+\sqrt{\lambda}}{s+s_1-s_2-\sqrt{\lambda}}. \tag{22}$$

In (19) the a stands for U, D, and in (20) for $UD, U\bar{U}$. The $p_n^a(ij), n = 0,1,2,3$ in (21) are polynomials of order n in s, s_1, s_2. A complete analytical result will be presented elsewhere [13]. Here we restrict ourselves to a comment and some numerical results. As may be seen from (19)–(21), the cumbersome interference functions contain inverse powers of λ (up to the third power), which vanish at the upper limit of integration over s_2. This is a typical example of so-called kinematical singularities. Expanding $\mathcal{L}_{3,4}$ in Taylor series in λ, one may see that all these inverse powers cancel and the cross-section has a proper threshold behaviour. However, these kinematical singularities may create complications for numerical calculations.

In figure 6, we present the ratios (basic+background)/(basic),

$$R = \frac{\sigma^{4f}(s)}{\sigma^{WW}(s)}, \tag{23}$$

for three different channels with 11, 10, and 9 diagrams respectively (see case (i) of table 1) as functions of $\sqrt{s}$. As is seen from the figure, the background contributions for these processes are relatively small, especially at LEP 2 energies. Below threshold of the W-production and at high energies, the relative contribution of such background increases and reaches $\sim 2\%$.

5 INITIAL STATE RADIATIVE CORRECTIONS IN FOUR-FERMION PRODUCTION PROCESSES

Since the background contribution is comparatively small, it is quite reasonable to restrict oneself to the basic diagrams when calculating the complete lowest-order ISR QED corrections.

Let us recall that the ISR corrections are known to be dominating in single Z-resonance production. A similar property holds for four-fermion processes at LEP 2, which will proceed near the corresponding $B_1 B_2$-thresholds and the intermediate-state bosons will be nearly at rest [14].

The ISR corrections for a cross-section described by s-channel diagrams with γ- and Z-exchanges (i.e. including the background terms) may be presented by a universal formula [15]- [16],

$$\sigma_{\text{univ}}^{B_1 B_2,s}(s) = \int_0^s ds_1 \rho_{B_1}(s_1) \int_0^{(\sqrt{s}-\sqrt{s_1})^2} ds_2 \rho_{B_2}(s_2)$$
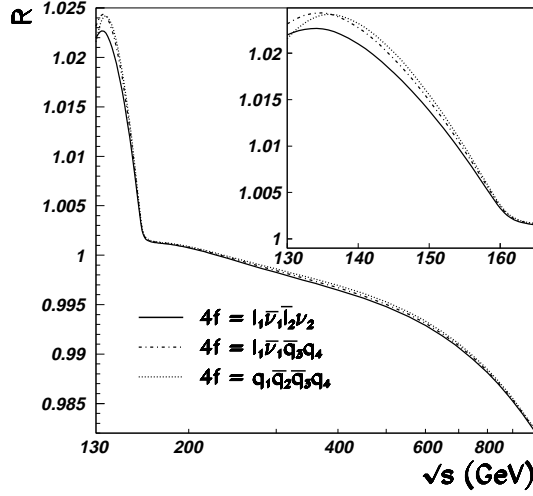
Figure 6: The (basic+background)/basic ratio R for off-shell W-pair production with $l_i \neq e$.

$$\int\limits_{(\sqrt{s_1}+\sqrt{s_2})^2}^{s} \frac{ds'}{s} \left[\beta_e v^{\beta_e - 1}(1 + \bar{S}) + \bar{H} \right]$$

$$\times \, \sigma_4^{B_1 B_2}(s'; s_1, s_2),$$

(24)

where $v = 1 - s'/s$. The soft plus virtual photon part $\bar{S}$ and the hard part $\bar{H}(s'/s)$ are given by

$$\bar{S} = \frac{\alpha}{\pi} \left[\frac{\pi^2}{3} - \frac{1}{2} \right] + \frac{3}{4}\beta_e + \mathcal{O}(\alpha^2), \tag{25}$$

$$\bar{H}(s'/s) = -\frac{1}{2}\left(1 + \frac{s'}{s}\right)\beta_e + \mathcal{O}(\alpha^2), \tag{26}$$

and $\beta_e = 2\alpha/\pi[\ln(s/m_e^2) - 1]$.

Equation (24) may be directly applied to the case $B_1 B_2 = ZH$ and to the s-channel contribution of $B_1 B_2 = WW$. We have rederived by explicit calculations that (24) may be obtained straightforwardly from the usual vertex and bremsstrahlung QED Feynman diagrams after up to seven sequential angular integrations (five for the vertex part and seven for bremsstrahlung). The situation becomes much more complicated if t- and u- channel exchange diagrams are involved. Here we face two kinds of problems. The factorized form (24) is no longer valid for the squared t- and u-channel diagrams and for st-,su-, and tu-interferences. One of the reasons is the angular dependence of t- and u-cha nnel propagators. This leads to the appearance of additional non-factorizable (non-universal) QED corrections.

For the ZZ process this is the only problem, although technical complications arise due to additional Feynman diagrams with real and virtual photons attached to the virtual

11

electron line in t- and u-channels. For the WW basic diagrams another problem persists. There, the electric charge flows from the initial state electron through an intermediate W-boson to a final state fermion. Therefore, only the complete set of all QED diagrams is gauge-invariant. A 'naïve' subset of diagrams with ISR corrections corresponding to the diagrams with a (real or virtual) photon attached to the external electron legs is not gauge-invariant. This is different from the ZZ basic diagrams, where the electric charge flows continuously through the initial state.

A straightforward solution of the problem would be a complete numerical calculation of *all* the $\mathcal{O}(\alpha)$ corrections, including also intermediate and final state corrections. This was done for the on-shell case in [17], but it seems to be incredibly complicated for the off-shell case (see [18]). In such a complete approach one must also include all electroweak corrections and properly treat the radiation from virtual intermediate $W^{\pm}$-states.

We used a completely different approach to the problem, namely to take advantage of the fact that ISR corrections should yield the main fraction of the net correction. Therefore, we tried to define a gauge-invariant ISR correction by splitting the electrically neutral neutrino flow in the t-channel into two oppositely flowing charges -1 and $+1$. The charge -1 is then combined with the 'naïve' ISR diagrams in order to build a continuous flow of electric charge in the initial state. The charge $+1$ is combined with the intermediate-state photon emission and is neglected here. This technique, which is explained in more detail in [14], is called the *Current Splitting Technique* (CST).

Within the CST, the ZZ and WW t-channel QED amplitudes are identical. The difference between the two cases arises at the level of cross-section calculations. For the WW case, there are st and tt interferences, while for the ZZ case one finds t- and u-channel contributions and the tu interference. In all cases the cross-section has the following structure:

$$\frac{d^3 \sigma_{\text{non}-\text{univ}}^{B_1 B_2,\text{a}}(s)}{ds_1 ds_2 ds'} = \frac{1}{s} \rho_{B_1}(s_1) \rho_{B_2}(s_2)$$
$$\times \left[\beta_e v^{\beta_e - 1} \mathcal{S}_{\text{a}} + \mathcal{H}_{\text{a}} \right], \tag{27}$$

with

$$\mathcal{S}_{\text{a}}(s, s'; s_1, s_2) = \left[1 + \bar{S}(s) \right] \sigma_0^{B_1 B_2,\text{a}}(s'; s_1, s_2)$$
$$+ \sigma_{\hat{S}}^{B_1 B_2,\text{a}}(s'; s_1, s_2), \tag{28}$$

$$\mathcal{H}_{\text{a}}(s, s'; s_1, s_2) = \bar{H}(s, s') \sigma_0^{B_1 B_2,\text{a}}(s'; s_1, s_2)$$
$$+ \sigma_{\hat{H}}^{B_1 B_2,\text{a}}(s, s'; s_1, s_2), \tag{29}$$

where $\sigma_{\hat{S}}^{B_1 B_2,\text{a}}(s'; s_1, s_2)$ and $\sigma_{\hat{H}}^{B_1 B_2,\text{a}}(s, s'; s_1, s_2)$ are non-universal, non-factorizable soft and hard contributions. Equation (27) possesses several remarkable properties. The leading ISR correction contributions to the cross-section, containing mass singularities via β_e, factorize for any $a = st, su, tu$-interferences and t- and u-channel exchanges. This is necessary to ensure that the gauge cancellation is not spoiled.

The non-universal terms are calculated so far only for the WW-case [14]. As one should expect, the non-universal contributions do not contain mass singularities. An analogous study for the ZZ case is in progress [19].

12

The numerical influence of the universal part of the ISR corrections (i.e. setting non-universal parts equal to zero) is presented in figures 3–5 for the WW, ZZ, and ZH cases. Universal ISR yields large, negative contributions in the vicinity of the threshold. At high energies these corrections are positive and one observes the effect of the radiative tail similar to the Z-peak. This radiative tail phenomenon is more pronounced than the high energy tail due to the bosons' off-shellness. We do not show the radiatively corrected on-shell cross-section $\sigma_{\mathrm{univ}}^{\mathrm{on}}$, but only mention that the relative differences between $\sigma_{\mathrm{Born}}^{\mathrm{on}}$ and $\sigma_{\mathrm{Born}}^{\mathrm{off}}$ on the one hand and between $\sigma_{\mathrm{univ}}^{\mathrm{on}}$ and $\sigma_{\mathrm{univ}}^{\mathrm{off}}$ on the other are similar.
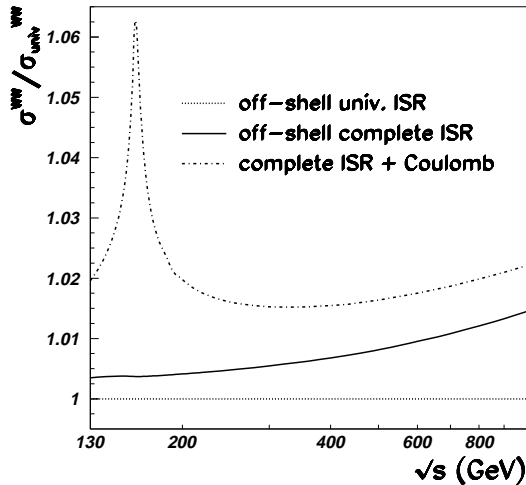

Figure 7: The non-universal initial state and Coulomb corrections to off-shell W-pair production.

The effect of the non-universal contributions in the WW-case is illustrated in figure 7 (solid line). This contribution is seen to be small, at LEP 2 energies it does not exceed 0.4%. At high energies the relative contribution of the non-universal term becomes as large as 1.4% at $\sqrt{s} = 1$ TeV. To a great extent the smallness of the non-universal terms at high energies is due to the *screening* property of the non-universal corrections. They have a damping overall factor,

$$\sigma_{\hat{S},\hat{H}}^{\mathrm{st,t}}\left(s';s_1,s_2\right) \sim \frac{s_1 s_2}{s^2}. \tag{30}$$

The screening property ensures the unitary behaviour of the non-universal terms at high energy for the individual (st and t) contributions.

In figure 7, we also show an important part of the final state corrections – the so-called Coulomb singularity. It yields a positive correction, which has its maximum value of about 6% at the threshold and vanishes at high energies. At $\sqrt{s}$=1000 GeV it amounts to 0.75%. The Coulomb correction is taken into account according to equation (5) of [20]. However, at high energies, other final state corrections are important [17].

6 CONCLUSIONS AND PROSPECTS

For a variety of purposes, the semi-analytical treatment of four-fermion production is an interesting alternative to the Monte Carlo approach.

Within the GENTLE project, we have calculated so far

(i) the $\mathcal{O}(\alpha)$ ISR corrections to and the average radiative energy loss $\langle E_{\mathrm{rad}} \rangle$ in off-shell W-pair production;

(ii) the background contribution for this process with the simplest final state configuration;

(iii) the off-shell ZH production with universal ISR corrections and the background contributions for the $\bar{\mu}\mu\bar{b}b$ decay mode.

We are presently studying

(iv) the $\mathcal{O}(\alpha)$ ISR corrections to off-shell Z-pair production.

We intend to study

(v) background contributions to Z- and W-pair production with other topologies;

(vi) background contributions with t-channel exchanges and final states with $e^{\pm}$ and ν_e or $\bar{\nu}_e$.

(vii) final state QED corrections to on-shell W-pair production with the current-splitting technique;

(viii) the inclusion of virtual weak corrections.

The annihilation of two particles into four (five particles in the case of real bremsstrahlung corrections) has a limited variety of topologies in the tree approximation for the basic process. Thus, its systematic treatment is of principal theoretical interest. Apart from the case of LEP 2, it finds additional applications in e.g. the study of the Z line shape at LEP 1 (initial state QED or final state QED and QCD higher order pair production corrections) or in QCD corrections at the LHC. A study of certain problems beyond the Standard Model is, of course, also within reach.

References

[1] O. Sushkov, V. Flambaum and I. Khriplovich, *Sov. J. Nucl. Phys.* **20** (1975) 537; W. Alles, Ch. Boyer and A. Buras, *Nucl. Phys.* **B119** (1977) 125.

[2] I.F. Ginzburg, G.L. Kotkin, S.L. Panfil and V.G. Serbo, *Nucl. Phys.* **B228** (1983) 285.

[3] T. Muta, R. Najima and S. Wakaizumi, *Mod. Phys. Letters* **A1** (1986) 203.

[4] A. Denner and T.Sack, *Z. Physik* **C45** (1990) 439.

[5] E. Boos et al., Proc. of the XXVIth Rencontres de Moriond, ed. J. Tran Than Van (Edition Frontieres, Paris, 1991), p. 501;
E. Boos et al., Proc. of the 2nd Int. Workshop on Software Engineering, ed. D. Perret-Gallix (World Scientific, Singapore, 1992), p. 665.

[6] D. Bardin, A. Leike and T. Riemann, these Proceedings.

[7] F.A. Berends, R. Pittau and R. Kleiss, INLO-PUB-1-94, and these Proceedings.

[8] D. Bardin, A. Leike, T. Riemann and M. Sachwitz, *Phys. Letters* **B206** (1988) 539.

[9] W. Beenakker and A. Denner, DESY 94-051 (1994).

[10] D. Bardin, M. Bilenky, A. Olchevski and T. Riemann, Fortran program GENTLE: A semi-Monte Carlo GENerator of the radiative Tail for LEP 200.

[11] J. Vermaseren, *Symbolic Manipulations with* FORM (Computer Algebra Nederland, Amsterdam, 1991).

[12] M. Veltman, SCHOONSCHIP – *A Program for Symbol Handling* (1989);
H. Strubbe, *Comp. Phys. Comm.* **8** (1974) 1.

[13] D. Bardin, M. Bilenky, A. Olchevski and T. Riemann, in preparation.

[14] D. Bardin, M. Bilenky, A. Olchevski and T. Riemann, *Phys. Letters* **B308** (1993) 403.

[15] F.A. Berends, G. Burgers and W.L. van Neerven, *Nucl. Phys.* **B297** (1988) 429;
B. Kniehl, M. Krawczyk, J.H. Kühn and R. Stuart, *Phys. Letters* **B209** (1988) 337.

[16] F.A. Berends, R. Pittau and R. Kleiss, INLO-PUB-6-94, and these Proceedings.

[17] W. Beenakker, K. Kolodziej and T. Sack, *Phys. Letters* **B258** (1991) 469;
J. Fleischer, K. Kolodziej and F. Jegerlehner, *Phys. Rev.* **D47** (1993) 830.

[18] A. Aeppli and D. Wyler, *Phys. Letters* **B262** (1991) 125;
A. Aeppli, BNL-46819 (1991) and contribution to: P.M. Zerwas (ed.), Proc. of the Workshop on Physics with e^+e^- Linear Colliders, DESY, 92-123A, August 1992;
G.J. van Oldenborgh, these Proceedings.

[19] D. Bardin, D. Lehner and T. Riemann, in preparation.

[20] D. Bardin, W. Beenakker and A. Denner, *Phys. Letters* **B317** (1993) 213.